Nanoparticles for Cancer Treatment

Role of Heat Transfer

C. Thomas Avedisian,[a] Richard E. Cavicchi,[b] Paul L. McEuen,[c] and Xinjian Zhou[c]

[a]*Sibley School of Mechanical and Aerospace Engineering, Cornell University, Ithaca, New York, USA*

[b]*Process Sensing Group, National Institute of Standards and Technology, Gaithersburg, Maryland, USA*

[c]*Department of Physics, Cornell University, Ithaca, New York, USA*

An overview is presented of an approach for treating cancer that uses nanoparticles to deliver heat to diseased areas after absorbing energy from a laser of the appropriate wavelength. The implications are discussed of the relationship of parameters necessary to raise the temperature to therapeutically beneficial levels. Tight focusing is required for a continuous-wave laser to sufficiently heat individual nanoparticles because of heat loss to the surrounding fluid during the period of exposure. The natural thermal confinement of pulse lasers minimizes this effect because of the finite thermal diffusion time, which restricts the absorbed energy to a region around the particle, that offers the potential for achieving high temperatures that can promote phase change on the surface of a nanoparticle or even melting of the particle. A discussion of a way to potentially measure temperature on the scale of an individual nanoparticle is included based on using a single-walled nanotube (SWNT) of carbon as a thermistor. The challenges of this undertaking are that SWNTs do not always follow Ohm's law, they may exhibit metallic or semiconductor behavior with an often unpredictable result in manufacturing, and no two SWNTs behave identically, which necessitates calibration for each SWNT. Some results are presented that show the electrical characteristics of SWNTs and their potential for exploitation in this application.

Key words: **cancer; nanoparticles; laser treatment; denaturation; thermal therapeutics; heat transfer**

Nomenclature

A	surface area
Bi	Biot number
c_p	specific heat
D	$= 2\,r_o$
D_o	incident beam diameter
f	focal length
f_N	particle concentration in mixture
g	gravitational constant (9.8 m/s^2 at Earth's surface)
h	heat transfer coefficient
k	thermal conductivity
L	cylinder length
Nu	Nusselt number
P_L	laser power
P''_L	laser flux at particle surface
Q_1	absorbed energy
Ra	Rayleigh number, $\frac{g\beta\Delta T r^3}{\alpha\nu}$
r_o	laser spot radius
r	radius
t	time
T_∞	far-field temperature
V	volume
α	fluid thermal diffusivity
β	thermal expansion coefficient
ΔT	$= T - T_\infty$

Address for correspondence: C. Thomas Avedisian, Cornell University, Sibley School of Mechanical and Aerospace Engineering, Upson and Grumman Halls, Ithaca, NY 14853-7501. cta2@cornell.edu

Interdisciplinary Transport Phenomena: Ann. N.Y. Acad. Sci. 1161: 62–73 (2009).
doi: 10.1111/j.1749-6632.2009.04090.x

δ	thermal diffusion length, $(\alpha t)^{1/2}$
ϕ	particle volume fraction
λ	laser wavelength
σ	absorption cross section
ρ	density
ν	fluid kinematic viscosity

Subscripts

l	individual particle
c	cylinder
f	fluid surrounding the particle or mixture
s	sphere
T	particle mixture

1. Introduction

Cancer is the second-leading cause of death among humans. Treatment possibilities include surgery, radiotherapy, and chemotherapy. Early work by Anderson and Parrish[1] showed the potential for a high-energy pulse laser to induce localized heating in tissue and cause cell damage when the temperature is raised above a threshold. The concept involved exposing a region of tissue to a pulse laser with a wavelength for which the diseased area had greater optical absorption than the surrounding tissue. The short duration of the laser pulse was further intended to confine the temperature increase to a region close to the particle as determined by the thermal diffusion length, which is on the order of $\delta \sim (\alpha t)^{1/2}$. Introduction of light-absorbing dye enhanced the concept by allowing more targeted heating.

The development of light-absorbing nanoparticles—solid particles of nanoscale dimensions—that are nontoxic to biological tissue has provided further potential for a more targeted delivery of heat with minimal damage to healthy tissue. At an appropriate wavelength, exposure of a nanoparticle to a laser can trigger a photothermal effect in the particle whereby electronic oscillations at the particle surface are converted to heat, which raises the particle temperature as determined by the particle's plasmon resonance. The resulting therapeutic effect is like a hyperthermia treatment but at the nanoscale. Other methods that can nonintrusively deliver heat include radiofrequency irradiation, ultrasound, and magnetic fields.[2–4]

When the particle gets comparatively hot, several effects are possible, such as denaturation of cells; alterations of the particle permeability to release materials encapsulated in or on the particle; and triggering bubble nucleation and growth on the surface of the particle, such that their rapid, and potentially explosive, collapse imparts a mechanical stress to diseased cells.[5–14] A variety of nanoparticles have been considered for this purpose, such as single-walled nanotubes (SWNTs) of carbon.[12] SWNTs are cylinders of nanometer diameter consisting of a single sheet of graphene wrapped up to form a tube[15], gold nanoshells,[7] pigmented particles,[5] gold nanoclusters,[8,9] and gold nanorods.[16] The nanoparticles must be nontoxic for the treatment to be effective and many of those developed for this purpose satisfy this requirement (gold is a good material in this regard).

The efficacy of treatment depends on the ability of the energy absorbers to locally heat diseased areas without damaging healthy tissue. An "optical window"[1] should exist whereby the particles are strongly absorbing at the wavelength of the laser, whereas the surrounding (healthy) tissue is relatively transparent. Only the particles and adjacent tissue are then heated if background absorption is negligible. This is the case for certain types of nanoparticles in the near infrared (NIR) in typical biological tissue where the nanoparticles are strongly absorbing, whereas tissue is relatively transparent (e.g., most animal tissues[12,17–21]). O'Neal *et al.*[21] and Oldenburg *et al.*[22] demonstrated a tunability for certain types of nanoparticles (e.g., silica cores with an ultrathin metallic gold coating), which arises by varying the thickness of the coating.

Temperature is the most important variable to control because temperature almost entirely determines the damage threshold for killing cells and the thermodynamic state of tissue

required to trigger a phase change (which under some conditions can be explosive, leading to the concept of a "nanobomb"[8,23]). Recent studies on nanoparticle–laser interactions have shown definite thermal effects of the laser on the average fluid state.[7,12] However, there is some question on the extent to which these effects can be localized to the scale of a single nanoparticle.[24]

This study addresses the heating process initiated by interaction of a particle with a laser with a simple model. A continuum is assumed (valid because the mean free path in liquids and amorphous solids is on the order of atomic distances[24]) and parameters are determined that can produce significant temperature changes localized to the nanoparticle, and yet it captures some of the effects of more complex models that have been developed for this process. The ability to measure temperature of an individual nanoparticle is important to test predictions, and the last section proposes an approach to do so based on developing an SWNT as a temperature sensor.

2. Modeling Laser Heating of Nanoparticles

Figures 1 and 2 show a schematic of the physical situation. A nanoparticle suspension is exposed to a laser at some focal distance f from the lens. The laser penetrates the fluid and is partly absorbed by the nanoparticles. A thermal zone is created in the fluid surrounding the particle or aggregate (as illustrated in Fig. 2) in which the absorbed heat is dissipated. For CW heating a steady state temperature is eventually reached due to the absorbed heat being balanced by heat dissipation to the surroundings. For pulse heating, higher temperatures can be reached, if only momentarily, depending on the pulse time because the heat dissipation rate limits the extent of cooling.

The extent to which a nanoparticle can be heated to produce a therapeutic effect, which typically means heated by 10 K or more, has

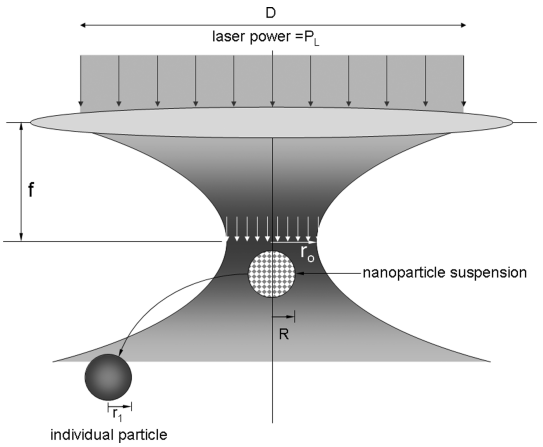

Figure 1. Schematic of laser–particle interaction where the nanoparticles are confined to a region *R*. The nanoparticle suspension is shown confined to a region R but in practice the nanoparticles may be dispersed over a wide zone. r_o is the focused beam spot size; f, the focal length; P_L, the laser power; and D, the incident beam diameter (not to scale). (In color in *Annals* online.)

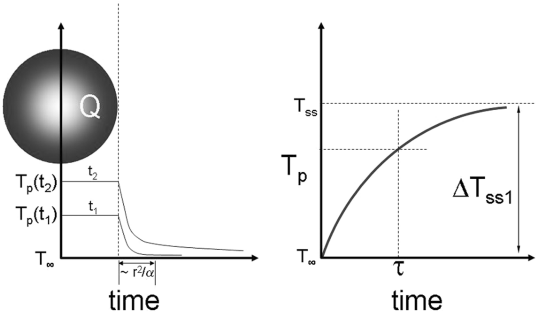

Figure 2. Schematic of the temperature distribution around a particle. (In color in *Annals* online.)

been estimated by detailed thermal models that consider a coupled particle–surrounding conduction domain with matching conditions at the interface and typically apply to pulse laser heating.[13,25,26] Predictions show that for certain conditions, heating by a pulse laser can produce very high particle temperatures that can exceed the bubble nucleation temperature and even the melting temperature of the particle. Such a situation is a consequence of the capability of certain pulse lasers to deliver high-energy pulses (e.g., $>10^8$ W/pulse) over times (nanoseconds to femtoseconds) whereby the energy absorbed by the particle is confined to the vicinity of the particle. At the other

end, continuous-wave (CW) lasers deliver much lower powers (e.g., order of 10 W) over far longer times, and significant dissipation occurs during the pulse, which limits the temperature increase. It is more challenging to employ a CW laser with the expectation of a significant temperature increase at the level of an individual particle. The following considers heating under CW conditions.

A simple heat transfer model that qualitatively captures some of the mechanisms for absorption and temperature increase is based on assuming that temperature gradients inside of a particle, or within an aggregate of particles, are negligible. This assumption is reasonable if the Biot number is small, $\mathrm{Bi}_1 = hr_1/k_1 \ll 1$ for a single particle or $\mathrm{Bi}_\mathrm{T} = h_\mathrm{T}\, r_\mathrm{T}/k_\mathrm{T} \ll 1$ for a particle/fluid mixture confined to a region r_T. Because heat transfer between the particle and surrounding medium is given by the Nusselt number, then if the same length scale is used to define both Bi and Nu (e.g., as for a sphere or long aspect ratio cylinder),

$$\mathrm{Bi}_{1,\mathrm{T}} \approx \mathrm{Nu}_{1,\mathrm{T}} \frac{k_\mathrm{f}}{k_{1,\mathrm{T}}}, \tag{1}$$

where $\mathrm{Nu}_{1,\mathrm{T}}$ is the Nusselt number between the volume where the laser energy is absorbed (particle or aggregate) and the surrounding medium. For spherical and cylindrical particles, the Nusselt number based on radius for natural convection from a sphere is of the form $\mathrm{Nu}_\mathrm{s} = 1.0 + f_\mathrm{s}$,[27] and for a long aspect ratio cylinder pertinent to an SWNT $\mathrm{Nu}_\mathrm{c} = 0.18 + f_\mathrm{c}$.[28] $f_{\mathrm{s,c}}$ is an empirical function of the Rayleigh (Ra) and Prandtl (Pr) numbers. The lead constants are the conduction limits for these geometries. If we take properties of water as typical (i.e., $k_\mathrm{f} \sim 0.63$ W/mK), a single particle with $r_1 < 100$ μm leads to $f_{\mathrm{s,c}} \ll 1$ so that $\mathrm{Nu}_\mathrm{c} = 0.18$ and $\mathrm{Nu}_\mathrm{s} = 1.0$. For $k_1 \sim 3000$ W/mK (SWNT[29]) or 318 W/mK (gold[30]), Eq. (1) shows that $\mathrm{Bi}_1 \ll 1$. For a larger volume of fluid confined in a cylindrical cuvette with the top surface exposed to air, an empirical correlation[30] shows that $\mathrm{Nu}_\mathrm{T} \sim 5$ when the conditions of Kam *et al.*[12] are used. On a volume fraction basis, a nanoparticle mixture will typically be dilute so that $k_\mathrm{T} \sim k_\mathrm{f}$. With $k_\mathrm{air} \sim 0.03$ W/mK, $\mathrm{Bi}_\mathrm{T} \ll 1$.

For a CW laser the appropriate energy balance equates the absorbed energy with the internal energy change of the particle and heat loss to the surroundings. The solution to this problem is

$$\Delta T_{1,\mathrm{T}} = b_{1,\mathrm{T}} \tau_{1,\mathrm{T}} \left(1 - e^{-t/\tau_{1,\mathrm{T}}}\right), \tag{2}$$

where $b_{1,\mathrm{T}} = \dfrac{Q_{1,\mathrm{T}}}{V_{1,\mathrm{T}} \rho_{1,\mathrm{T}} C_{p_{1,\mathrm{T}}}}$, and the time constant is

$$\tau_{1,\mathrm{T}} = \frac{V_{1,\mathrm{T}} \rho_{1,\mathrm{T}} r_{1,\mathrm{T}}}{\mathrm{Nu}_{1,\mathrm{T}} k_\mathrm{f} A_{1,\mathrm{T}}}. \tag{3}$$

The steady-state temperature ($t \to \infty$) is

$$\Delta T_{1,\mathrm{T}} = \frac{Q_{1,\mathrm{T}} r_{1,\mathrm{T}}}{\mathrm{Nu}_{1,\mathrm{T}} A_{1,\mathrm{T}} k_\mathrm{f}}. \tag{4}$$

The energy absorbed in a single particle is $Q_1 = P''_\mathrm{L}\, \sigma$, where σ (m^2) is the absorption cross section. For a mixture with particle concentration of f_N in a volume V_T, $Q_\mathrm{T} = Q_1 f_\mathrm{N} V_\mathrm{T}$. In terms of the volume fraction, ϕ, Eq. (4) can also be written as $\Delta T_\mathrm{T} = \phi \frac{Q_1 R_\mathrm{T}}{\mathrm{Nu}_\mathrm{T} A_1 k_\mathrm{f}}$, which gives the ratio of solution temperature to individual particle temperature as $\frac{\Delta T_\mathrm{s}}{\Delta T_1} = \phi \frac{r_\mathrm{T}}{r_1}$.

To place the preceding development in some context, we will estimate the temperature of an individual particle and a solution by using Eq. (4) for heating by a CW laser. The experimental conditions are a suspension of gold nanoshells and an SWNT mixture. For nanoshells, Hirsch *et al.*[7] report that $\sigma = 3.8 \times 10^{-14}$ m^2, $f_\mathrm{N} = 4.4 \times 10^{15}$ m^{-3}, $P''_\mathrm{L} = 35 \times 10^4$ W/m^2, and $r_1 = 65$ nm. If we use $\mathrm{Nu}_1 = 1$ as noted previously, Eq. (4) gives $\Delta T_1 \approx 0.0054$ K, which is too small for any biological benefit. Similarly, the SWNT mixtures of Kam *et al.*,[12] for which $P''_\mathrm{L} = 1.4 \times 10^4$ W/m^2, $\rho_1 \sim 1400$ kg/m^3 (SWNT density), $L_1 \sim 150$ nm, $r_1 \sim 0.6$ nm, $k_\mathrm{f} \sim 0.63$ W/mK

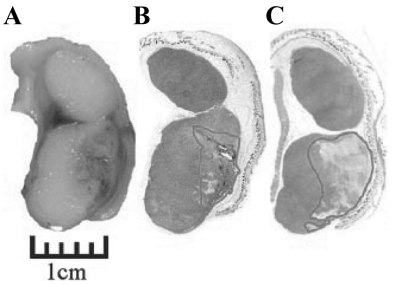

Figure 3. Magnetic resonance thermal imaging images of mice tissue showing irreversible damage.[7] (**A**) Overall view of tissue, (**B**) region of localized nanoshells in red, and (**C**) area showing tissue damage after exposure. (In color in *Annals* online.)

(water), and $\sigma = 1.31 \times 10^{-18}$ m^2 (based on their reported molar extinction coefficient of 7.9×10^6 M^{-1} cm^{-1}), lead to $\Delta T \sim 10^{-5}$ K from Eq. (4). As a result, individual particles cannot be sufficiently heated by a CW laser under these conditions. Yet, significant temperature increases have been measured for nanoparticle aggregate mixtures in water. For example, Figure 3 shows tissue damage that resulted from exposure of a mouse that had been inoculated in its hind legs with canine transmissible venereal tumor cells that were grown to tumors.[7] A solution of nanoshells was then injected into the tumor and the region exposed to an NIR laser source. Significant tissue damage was observed only where the nanoshells existed, as shown in Figure 3. Equally important, magnetic resonance thermal imaging of the tissue showed significant temperature increases that correlated with the observed cell damage. These results are explained by considering the aggregate when estimating the temperature increase.

For the *in vitro* experiments of Hirsch *et al.*[7] that used a particle concentration of 4.4×10^{15}, Eq. (4) shows that $\Delta T_{\mathrm{T}} \sim 46$ K, which is the right order of magnitude compared to the measurements. The SWNT suspensions studied by Kam *et al.*[12] were more concentrated at 2.9×10^{19} m^{-3}. The energy loss from their nanoparticle mixture confined in a 3-cm diameter by a 1-cm-high cuvette is assumed to occur only from the top surface to air. For this case, $\mathrm{Nu}_{r_{\mathrm{T}}} = 0.54\,\mathrm{Ra}_{r_{\mathrm{T}}}^{1/4}$ (see Ref. 30) may be an appropriate correlation, where $r_{\mathrm{T}} = 1.5$ cm. The computed SWNT molecular weight for a 150-nm-long by 1.6-nm-diameter SWNT is 520 kg/mole. The steady-state temperature rise predicted by Eq. (4) for an incident heat flux of 1.4 W/cm^2 is about 346 K. The actual mixture temperature will of course not reach this value because other processes will be triggered at lower temperatures that are not included in the lumped capacitance model, such as nucleate boiling, which was noted by Kam *et al.*[12] for exposure times longer than 2 min. Bubble nucleation triggered by pulse-heating nanoparticle suspensions has also been experimentally demonstrated.[8,9,26,31]

To further show the effect of a CW laser on the temperature of a solution of nanoparticles, we measured the temperature increase of a suspension of 10-nm-diameter gold spheres confined in an optically transparent cuvette (type 9P cuvette; NSG Precision Cells, Inc.). The experimental arrangement is shown in Figure 4. Temperature was measured at a reference location in the cuvette to provide a qualitative measure of the effect of the laser. A 75-μm-diameter thermocouple (Omega #5SC-TT-K-40-12) was positioned along the centerline of the cuvette so that the bead was approximately 3.2 mm above the centerline of the beam and out of the beam path (with the fluid removed from the cuvette and with the thermocouple in place and the laser turned on, the temperature remained at the ambient value). The laser was a Spectra-Physics diode laser (#BWA-0500-808-10-01) at a wavelength of 808 nm, controlled by a #5600-20 driver, #3150 temperature controller, and #763H-FC heat sink, which irradiated a 3-mm-diameter spot of the front face of the cuvette. Concentrations of 5.7×10^{10} mL^{-1}, 5.7×10^{11} mL^{-1}, 5.7×10^{12} mL^{-1}, and 5.7×10^{13} mL^{-1} were examined, which corresponded to volume fractions of 1.8×10^{-13}, 1.8×10^{-12}, 1.8×10^{-11}, and 1.8×10^{-10}, in addition to pure water. The laser power was set at 7.4 W (corresponding to a driver current of 10 A) and the laser was kept

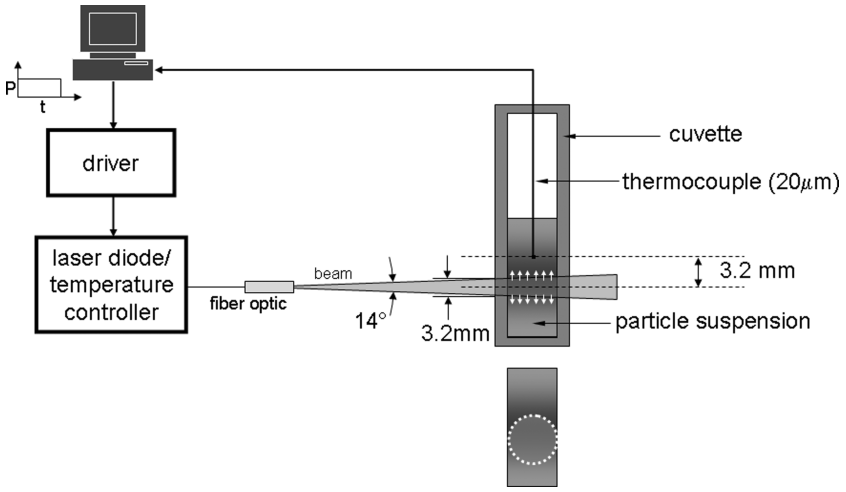

Figure 4. Schematic of apparatus for measuring temperature at a reference position in a NIR-irradiated nanosphere suspension. (In color in *Annals* online.)

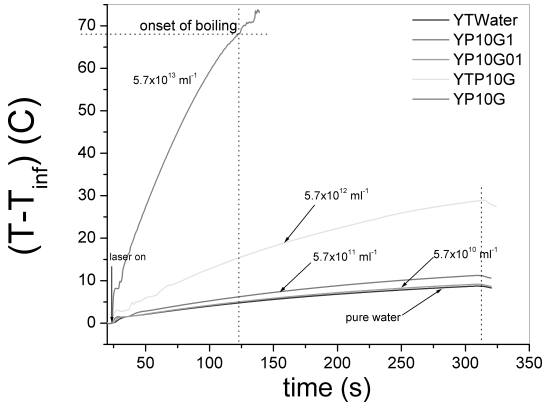

Figure 5. Variation of temperature increase of the indicated particle concentrations of gold nanosphere suspensions due to irradiation of a 7.4-W, 325-s pulse of an NIR laser. Boiling occurs at highest concentration. (In color in *Annals* online.)

on for 325 s. The laser was controlled through a LABView program and the thermocouple output was stored on a computer through an electronic cold junction.

As shown in Figure 5, temperature oscillations were observed immediately after the laser was turned on. This behavior suggests a stabilization of the temperature gradient in the solution (perhaps by convective motion) followed by a monotonic increase in temperature for the rest of the heating period. Interestingly, pure water showed measurable background heating, indicating that water is not completely transparent at 808 nm. At the highest concentration of gold nanoparticles (5.7×10^{13} mL^{-1}) the temperature reached nearly 100°C at 125 s and boiling in the cuvette was observed.

The temperature increases shown in Figure 5, as well as those previously reported,[7,12] confirm the ability of dilute concentrations of absorbing nanoparticles to produce significant temperature increases of therapeutic value. The substantial effects shown in Figure 5 cannot be explained on the basis of localized heating at the scale of nanoparticles as indicated previously for CW heating and must be the result of a more collective effect of absorption and dissipation of energy by the aggregate of particles.

To estimate the temperature rise of our gold nanosphere solutions, we assume that at the highest concentration, absorption of the incident laser power will be dominated by nanoparticles and that any background effect from water will be small. This assumption would not be correct for very dilute concentrations, and for that reason we apply Eq. (4) only to the highest concentration examined and assume that σ for a gold nanosphere entirely determines the absorbed energy. The geometry of the heated

volume is a cylinder defined by the laser beam (i.e., 3-mm diameter, 1 cm long [Fig. 4]) that passes through the cuvette in a surrounding medium of the same material (i.e., k_f is the same for the heated volume and surroundings). The incident power is assumed to be uniform over the 3-mm spot size, and $Nu_T \sim 0.18$ even though the cylinder of fluid traced by the laser beam is not in an infinite medium. Because we are interested primarily in a qualitative estimate, this assumption will suffice here. From Mie scattering theory and if we account for the refractive index of the surrounding water, $\sigma \approx 2.4 \times 10^{-19}$ m^2 for 10-nm gold spheres at a wavelength of 808 nm. From Eq. (3) the predicted time constant is $\tau_T \sim 50$ s and the temperature rise from Eq. (4) is $\Delta T_1 \approx 149$ K. These estimates are remarkably close to the measurements in Figure 5 for the highest concentration, considering the uncertainty of the input parameters and the simplicity of the model. Adjusting input parameters even slightly (e.g., absorption cross section, Nusselt number) could improve agreement and allow a more quantitative prediction.

The preceding examples show that for the given conditions a CW laser with its limited power and pulse limitations cannot generally produce temperature increases at the scale of a nanoparticle itself; on the other hand, aggregates can be substantially heated. At the level of an individual nanoparticle, $P''_L = P_L/(\pi r_o^2)$, and if we take an SWNT with length L_1 and radius r_1 as an example, Eq. (4) can be expressed in terms of the required laser spot size as $r_o = (\frac{P_L \sigma r_1}{\pi \, Nu_{r_1} \, k_f A_1 \Delta T_1})^{1/2}$. The absorption cross section for an SWNT was estimated from the bare optical cross section[32] as $\sigma' = 70$ m^2/moleC so that $\sigma = n_c \sigma'$, where n_c is the number of moles of carbon atoms in an SWNT. The distance between adjacent carbon atoms in a parallelogram unit cell of a 2-D graphene sheet is 0.142 nm and the area of the unit cell, A_{cell}, is 0.026 nm^2. The unit cell contains two carbon atoms. The number of moles of carbon atoms in a SWNT is then $n_c = 2A_{swnt}/(A_{cell}A_v)$, where

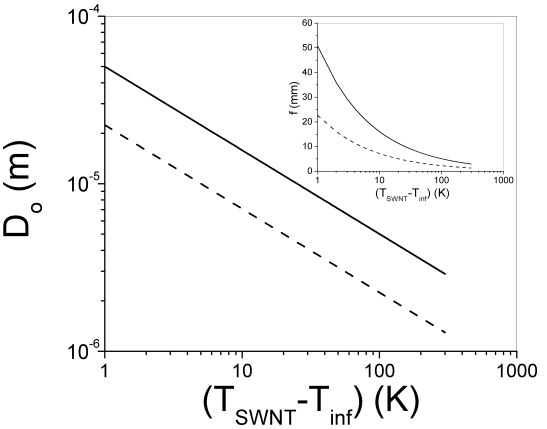

Figure 6. Required laser spot size (diameter) to reach the indicated temperature increase for a 1-nm and 5-nm diameter by 10-μm-long SWNT exposed to an 808-nm, 10-W CW laser. Dotted line, 1-nm-diameter SWNT; solid line, 5-nm-diameter SWNT. Inset, diffraction-limited focal length for 808-nm light.

A_v is Avogadro's number and A_{swnt} is the surface area of a single SWNT. With $L_1 \approx 10$ μm, which is a length that will facilitate development of an SWNT into a temperature sensor (see Section 4), the absorption cross section is approximately $\sigma \approx 5.62 \times 10^{-14}$ m^2 for a 1-nm-diameter SWNT and $\sigma \approx 2.81 \times 10^{-13}$ m^2 for a 5-nm-diameter SWNT.

Figure 6 shows the predicted temperature rise of a single SWNT for $P_L = 10$ W in water ($k_f \sim 0.6$ W/mK) up to $\Delta T = 300$ K, which covers bubble nucleation at the superheat limit.[33] Such a process has been considered in laser pulse heating of nanoparticle solutions, a consideration previously noted.[8,9,26,34,35] Also shown in the inset of Figure 6 is the diffraction-limited focal length, $f = \frac{1}{1.22} \frac{D_o D}{\lambda}$. Only focal lengths smaller than shown in the inset to Figure 6 (for a given SWNT diameter) are permissible. The predicted focal lengths generally do not pose significant experimental difficulties except at the highest temperatures.

A feature of nanoparticles is their potential to deliver localized energy to surrounding tissue. A test of such a capability for given parameters requires measuring temperature on the scale of the particle itself. We next discuss this matter.

3. Nanothermometry with a Nanotube

The ability to directly measure temperature of an individual nanoparticle requires spatially resolving to that scale. Commercially available thermocouples are too large. Laser-based methods have the potential for more localized temperature measurement, with a diffraction-limited spatial resolution of about 1 μm in the NIR. The temperature is an average over the particles within the measurement volume. For example, experiments to measure the vibrational response of nanoparticles pulse-heated in a 2×10^{-4} M solution of gold nanoparticles[26,31,36] were used to infer temperature through the relationship between the fundamental breathing mode of vibration and the particle's speed of sound, which is temperature dependent. The effective laser spot size was more than 100 μm. A probe volume corresponding to this spot size would contain more than 10^{11} particles. Similar considerations apply to other laser methods for temperature measurement.[11,37]

A direct measurement of temperature at the scale of an individual isolated nanoparticle does not appear to have been done. One concept that may have promise for this purpose is based on thin-film thermometry, which infers temperature from a measurement of electrical resistance through a calibration of electrical resistance with temperature. The idea is to transform the nanoparticle itself into a resistance thermometer for nanoparticles that can carry current. The challenges include identification of a suitable geometry for the particle to facilitate the measurement, integrating the particle into an electronic package to which appropriate interfacing with instrumentation can be made for electrical measurements, and ensuring that the particle has a sufficiently strong variation of resistance with temperature to make viable an accurate measurement of temperature.

When we consider the various geometries of nanoparticles that have been fabricated—rod, cylinder, sphere—the cylinder is the most convenient to develop into a sensor. SWNTs fit this requirement. SWNTs are somewhat long along their axes (order of micrometers) but have diameters that can be as small as 1 nm. In this sense the temperature of an SWNT could provide information on a nanoscale as it relates to the SWNT diameter. The electrical resistivity of individual SWNTs can have a reasonably strong dependence on temperature, though this information comes from data at room temperature or lower.[38,39] The thermal and electrical characteristics of individual SWNTs at high temperatures are largely unexplored, and the trends at low temperature cannot be extrapolated to temperatures of interest. The technology for fabricating electronic packages of individual SWNTs that bridge metal electrodes exists.[41–46] The configurations have included SWNTs freely suspended or lying on a substrate. Substrate-supported SWNTs may have greater structural integrity than that of SWNTs that bridge electrodes across a trench (i.e., suspended SWNT) and may be less prone to burnout because of increased heat sinking of the SWNT through the substrate[47] and their larger current-carrying capability.[48] In the following we present some results for substrate-supported SWNTs that suggest their potential for measuring temperature significantly above room temperature.

The small size of SWNTs motivated an integrated fabrication process in which SWNTs were grown across metal (i.e., gold) electrodes and which was in direct contact with the substrate across the electrodes (i.e., silicon). The process is described elsewhere.[15,43,49] The fabrication process begins with an Si wafer that is degeneratively doped with a 500-nm layer of SiO_2. A 50-nm metal layer of Au is then evaporated on top of the SiO_2. FeO_3/MoO_2 catalyst pads are photolithographically patterned on the Au. The assembly is then placed in a chemical vapor deposition furnace with a constant flow of methane to grow the nanotube. The SWNTs grow from pad to pad with the aid of a wet etching step in buffered oxide. After etching, a drying step is performed to prevent

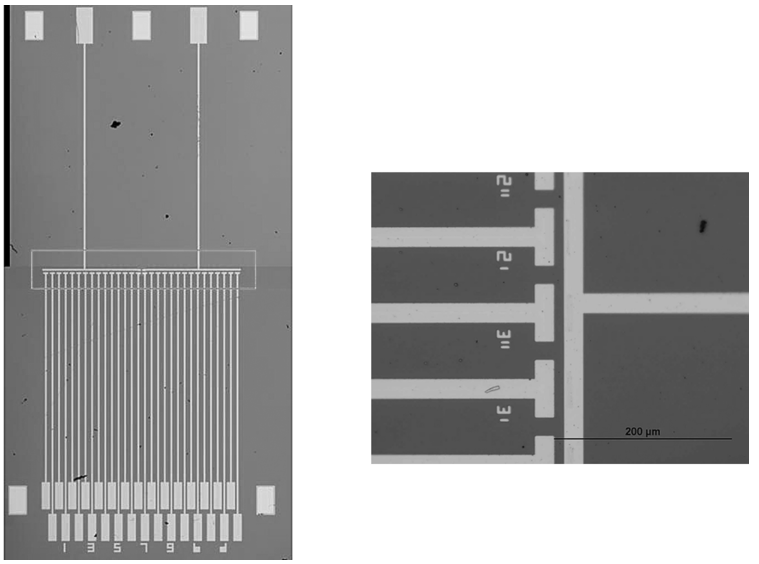

Figure 7. Photomicrograph of a nanotube package. Numbered pads at the bottom and two pads at the top are contacts for measuring the bias voltage. The other pads (without lines) are gate voltage pads. Nanotubes (not visible) are grown across the gap within the zone marked by the green rectangle. Visible metallization is Au and the substrate is Si. Some of the packages had a Cr underlayer for enhanced adhesion. (In color in *Annals* online.)

the SWNT from sticking to the substrate. With this method, a package that contains one or a few nanotubes can be created. It is not possible to know how many SWNTs are grown across the metallic pads until a current is measured for a given bias voltage. The result is an SWNT that bridges across the electrodes and that is in direct contact with the substrate between the electrodes.

Figure 7 is a photomicrograph of a typical electronic package used in our measurements. The metallization pattern is shown by the bright yellow (gold) lines. The lines terminate in tees, across which the SWNTs are grown. Provision in the package was made for varying the gate voltage to investigate the electrical characteristics of SWNTs in an electric field. In the experiments reported here, the gate voltage was zero. The SWNT diameters ranged from 1 nm to 5 nm and were about 10–12 µm long. Some of the packages also included a 50-nm sublayer of Cr, which provided enhanced adhesion of the gold. Without the Cr layer, the pads for electrical contact were fragile and often tended to scratch on the probe station during measurements.

After fabrication, the packages are annealed in an oven at 400–600°C by an "ashing" procedure to improve (lower) the contact resistance (R_c) and clean the surface of residues associated with processing. The concern with contact resistance was recently addressed,[42,43,48] in which it was pointed out that platinum and gold electrodes provide lower contact resistance than other metals. Typically, R_c would be about an order of magnitude less than the resistance of the SWNT.[40,48,50–52] Electrical connections to the pads shown in Figure 6 were made by probe station contacts. A hot plate was integrated with the probe station to allow temperature control of the SWNT.

The procedure for measuring electrical resistance was to slowly vary the temperature of the hot plate from room temperature to about 300°C—to our knowledge, the highest temperature at which the electrical characteristics of SWNTs have been measured. At each temperature, current through an SWNT was measured by scanning voltage from −2 V to +2 V under LABView control. An example of one voltage scan in air is shown in Figure 8.[51] The measurements were repeatable for a given SWNT. The

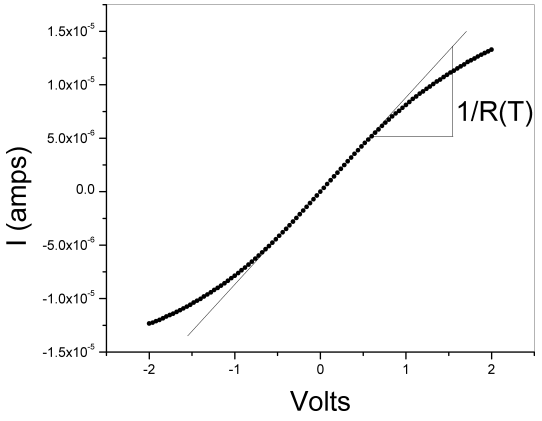

Figure 8. Variation of current with voltage of an SWNT. The linear portion around $V = \pm 0.5$ V determines the resistance.

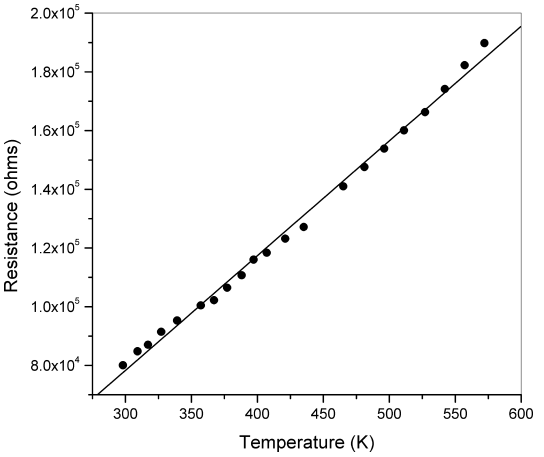

Figure 9. Variation of electrical resistance with temperature for an SWNT. Resistance was determined from linear portion of I–V behavior typical of Figure 8.

relationship between current and voltage was linear only around the origin (±0.5 V), suggesting an Ohmic behavior. In this range the resistance was determined (i.e., inverse slope of the I–V [current–voltage] characteristic). Noticeable nonlinearities existed at higher bias voltages, which indicate non-Ohmic behavior that may be due to scattering of optical phonons[48] or possibly self-heating effects.[46]

The variation of electrical resistance (inverse slope of the linearized data in Fig. 8) with temperature is shown in Figure 9.[51] Over the temperature range indicated, the variation of electrical resistance with temperature is reasonably linear for this particular SWNT, with nominal values in the range of several hundred kiloohms, though as noted previously the quantitative measurements shown in Figure 8 would not apply to a different SWNT. Kane *et al.*[53] recently reported an extensive study of the effect of processing history and nature of the electrode connection on resistance of SWNTs in a vacuum. It was shown that species which may be absorbed on SWNTs could be removed by heat-treating them which appears to lead to a linear variation of electrical resistance with temperature. Lead (Pb) contacts were shown to have an especially strong effect on the contact resistance. With such a SWNT as shown in Figure 8, it is in principle possible to use the trend to infer temperature upon exposure to a laser with appropriate parameters from measurement of the electrical resistance of the SWNT by incorporating an SWNT into a suitable bridge circuit. This is an effort for continuing research.

6. Conclusions

Laser heating of nanoparticle suspensions can produce temperature increases localized to the scale of the nanoparticle, provided that laser parameters are appropriately adjusted. Heating by a CW laser produces a steady-state temperature, which may have a therapeutic effect for sufficiently tight focusing. Pulse lasers derive their benefit from thermal confinement, in which the energy absorbed by a nanoparticle is not sufficiently dissipated during the pulse, which can produce temperatures exceeding the superheat limit of the surrounding fluid and even the melting temperature of the particle.

A direct measurement of the local temperature that results from optical heating is challenging. Laser-based methods provide a temperature averaged over the particles within the laser probe volume, which can contain an enormous number of nanoparticles. Fashioning an SWNT into a sensor offers the capability of a direct nanoscale temperature measurement relative to the diameter of the SWNT. The SWNT electrical resistance exhibits a positive slope above room temperature up to 300°C, which

suggests its use as a thermistor. The electrical characteristics are unique to each SWNT and would have to be measured individually. The non-Ohmic behavior of SWNTs at high bias voltages restricts the range over which measurements of voltage and current can be used to determine electrical resistance as a function of temperature.

Acknowledgments

This work was supported by the New York State Office of Science, Technology, and Academic Research with Dr. Kelvin Lee as the Director. We thank Dr. Joseph T. Hodges for providing a Mie scattering prediction of the absorption cross section of a gold nanosphere and Dr. Leonard Pease for providing the gold nanofluid solutions. The laboratory assistance of Mr. Johannes Kutten is acknowledged. We also thank Dr. Michael J. Tarlov of the National Institute of Standards and Technology for his interest in our work.

Conflicts of Interest

The authors declare no conflicts of interest.

References

1. Anderson, R.R. & J.A. Parrish. 1983. Selective photothermolysis: precise microsurgery by selective absorption of pulsed radiation. *Science* **220:** 525–527.
2. Miller, D.L., G.J.R. Spooner & A.R. Williams. 2001. Photodisruptive laser nucleation of ultrasonic cavitation for biomedical applications. *J. Biomed. Optics* **6:** 351–358.
3. Hilger, I., R. Hergt & W.A. Kaiser. 2005. Towards breast cancer treatment by magnetic heating. *J. Magnetism Magnetic Mat.* **293:** 314–319.
4. Gannon, C.J., P. Cherukuri, B.I. Yakobson, *et al*. 2007. Carbon nanotube-enhanced thermal destruction of cancer cells in a noninvasive radiofrequency field. *Cancer* **110:** 2654–2665.
5. Lin, C.P., M.W. Kelley, A.B. Sibayan, *et al*. 1999. Selective cell killing by microparticle absorption of pulsed laser radiation. *IEEE J. Quantum. Elec.* **5:** 963–968.
6. Brinkmann, R., G. Huttmann, J. Rogener, *et al*. 2000. Origin of RPE-cell damage by pulsed laser irradiance in the ns to μs time regime. *Lasers Surg. Med.* **27:** 451–464.
7. Hirsch, L.R., R.J. Stafford, J.A. Bankson, *et al*. 2003. Nanoshell-mediated near-infrared thermal therapy of tumors under magnetic resonance guidance. *Proc. Natl. Acad. Sci. USA* **100:** 13549–13554.
8. Zharov, V.P., R.R. Letfullin & E.N. Galitovskaya. 2005. Microbubbles-overlapping mode for laser killing of cancer cells with absorbing nanoparticle clusters. *J. Phys. D Appl. Phys.* **38:** 2571–2581.
9. Zharov, V.P., E.N. Galitovskaya, C. Johnson & T. Kelly. 2005. Synergistic enhancement of selective nanophotothermolysis with gold nanoclusters: potential for cancer therapy. *Lasers Surg. Med.* **37:** 219–226.
10. Kotaidis, V., C. Dahmen, G.V. Plessen, *et al*. 2006. Excitation of nanoscale vapor bubbles at the surface of gold nanoparticles in water. *J. Chem. Phys.* **124:** 184702.
11. Skirtach, A.G., C. Dejugnat, D. Braun, *et al*. 2005. The role of metal nanoparticles in remote release of encapsulated materials. *Nano Lett.* **5:** 1371–1377.
12. Kam, N.W.S., M. O'Connell, J.A. Wisdom & H. Dai. 2005. Carbon nanotubes as multifunctional biological transporters and near-infrared agents for selective. *Proc. Natl. Acad. Sci. USA* **102:** 11600–11605.
13. Khlebtsov, B., V. Zharov, A. Melnikov, *et al*. 2006. Optical amplification of photothermal therapy with gold nanoparticles and nanoclusters. *Nanotechnology* **17:** 5167–5179.
14. Zharov, V.P., K.E. Mercer, E.N. Galitovskaya & M.S. Smeltzer. 2006. Photothermal nanotherapeutics and nanodiagnostics for selective killing of bacteria targeted with gold nanoparticles. *Biophys. J.* **90:** 619–672.
15. McEuen, P.L., M.S. Fuhrer & H. Park. 2002. Single-walled carbon nanotube electronics. *IEEE Trans. Nanotech.* **1:** 78–85.
16. Huang, X., I.H. El-Sayed, W. Qian & M.A. El-Sayed. 2006. Tunable infrared absorption by metal nanoparticles: the case for gold rods and shells. *J. Am. Chem. Soc.* **128:** 2115–2120.
17. West, J.L. & N.J. Halas. 2000. Applications of nanotechnology to biotechnology. *Curr. Opin. Biotech.* **11:** 215–217.
18. König, K. 2000. Multiphoton microscopy in life sciences. *J. Microsc.* **200**(Pt 2): 83–104.
19. Weissleder, R. 2001. A clearer vision for in vivo imaging. *Nat. Biotechnol.* **19:** 316–317.
20. Cherukuri, P., S.M. Bachilo, S.H. Litovsky & R.B. Weisman. 2004. Near-infrared fluorescence microscopy of single-walled carbon nanotubes in phagocytic cells. *J. Am. Chem. Soc.* **126:** 15638–15639.
21. O'Neal, D.P., L.R. Hirsch, N.J. Halas, *et al*. 2004. Photo-thermal tumor ablation in mice using near

infrared-absorbing nanoparticles. *Cancer Lett.* **209:** 171–176.
22. Oldenburg, S.L., R.D. Averitt, S.L. Westcott & N.J. Halas. 1998. Nanoengineering of optical resonances. *Chem. Phys. Lett.* **28:** 243–247.
23. Panachapakesan, B., L. Shaoxin, K. Sivakumar, *et al*. 2005. Single-wall carbon nanotube nanobomb agents for killing breast cancer cells. *NanoBiotech.* **1:** 133–139.
24. Keblinski, P., D.G. Cahill, A. Bodapati, *et al*. 2006. Limits of localized heating by electromagnetically excited nanoparticles. *J. Appl. Phys.* **100:** 054305.
25. Pitsillides, C.M., E.K. Joe, X. Wei, *et al*. 2003. Selective cell targeting with light-absorbing microparticles and nanoparticles. *Biophys. J.* **84:** 4023–4032.
26. Hartland, G.V. 2004. Measurements of the material properties of metal nanoparticles by time-resolved spectroscopy. *Phys. Chem. Chem. Phys.* **4:** 5263–5274.
27. Churchill, S.W. 2002. Free Convection around Immersed Bodies. In *Heat Exchanger Design Handbook*. G.F. Hewitt Ed.: Section 2.5.7. Begell House. New York.
28. Churchill, S.W. & H.H.S. Chu. 1975. Correlating equations for laminar and turbulent free convection from a vertical plate. *Int. J. Heat Mass Transf.* **18:** 1323.
29. Kim, P., L. Shi, A. Majumdar & P.L. McEuen. 2001. Thermal transport measurements of individual multiwalled nanotubes. *Phys. Rev. Lett.* **87:** 215502.
30. Incropera, F.P., D.P. DeWitt, T.L. Bergman & A.S. Lavine. 2007. *Introduction to Heat Transfer*. 5th edition, p. 541, Appendix A. John Wiley. New York.
31. Hu, M. & G.V. Hartland. 2002. Heat Dissipation for Au Particles in Aqueous Solution: Relaxation Time versus Size. *J. Phys. Chem.* **106:** 7029–7033.
32. Murakami, Y., E. Einarsson, T. Edamura & S. Maruyama. 2005. Polarization dependence of the optical absorption of single-walled carbon nanotubes. *Phys. Rev. Lett.* **94:** 087402.
33. Avedisian, C.T. 1985. The Homogeneous nucleation limits of liquids CT avedisian. *J. Phys. Chem. Ref. Data* **14:** 695–720.
34. Neumann, J. & R. Brinkmann. 2007. Nucleation dynamics around single microabsorbers in water heated by nanosecond laser irradiation. *J. App. Phys.* **101:** 114701.
35. Lapotko, D.O., T.R. Romanovskaya, A. Schnip & V. Zharov. 2002. Photothermal time-resolved imaging of living cells. *Lasers Surg. Med.* **31:** 53–63.
36. Petrova, H., M. Hu & G.V. Hartland. 2007. Photothermal properties of gold nanoparticles. *Z. Phys. Chem.* **221:** 361–376.
37. Richardson, H.H., Z.N. Hickman, A.O. Govorov, *et al*. 2006. Thermooptical properties of gold nanoparticles embedded in ice: characterization of heat generation and melting. *Nanoletters* **6:** 738–788.
38. Fischer, J.E., H. Dai, A. Thess, *et al*. 1997. Metallic resistivity in crystalline ropes of single-wall carbon nanotubes. *Phys. Rev. B.* **55:** R4921–R4924.
39. Kane, C.L., E.J. Mele, R.S. Lee, *et al*. 1998. Temperature-dependent resistivity of single-wall carbon nanotubes. *Europhys. Lett.* **41:** 683–688.
40. Franklin, N.R., Q. Wang, T.W. Tombler, *et al*. 2002. Integration of suspended carbon nanotube arrays into electronic devices and electromechanical systems. *Appl. Phys. Lett.* **81:** 913–915.
41. Mann, D., A. Javey, J. Kong, *et al*. 2003. Ballistic Transport in Metallic Nanotubes with Reliable Pd Ohmic Contacts. *Nano Lett.* **3:** 1541–1544.
42. Mann, D., K.E. Pop, J. Cao, *et al*. 2006. Thermally and molecularly stimulated relaxation of hot phonons in suspended carbon. *Phys. Chem. B* **110:** 1502–1505.
43. Cao, J., Q. Wang, D. Wang & H. Dai. 2005. Suspended carbon nanotube quantum wires with two gates. *Small* **1:** 138–141.
44. Cao, J., Q. Wang, M. Rolandi & H. Dai. 2004. Aharonov-bohm interference and beating in single-walled carbon-nanotube interferometers. *Phys. Rev. Lett.* **93:** 216803. nyas_04090 nyas2009-v1.cls (1994/07/13 v1.2u Standard LaTeX document class) 1-30-2009:956
45. Javey, A., J. Guo, Q. Wang, *et al*. 2003. Ballistic carbon nanotube field-effect transistors. *Nature* **424:** 654–657.
46. Heller, I., J. Kong, H.A. Heering, *et al*. 2005. Individual single-walled carbon nanotubes as nanoelectrodes for electrochemistry. *Nano Lett.* **5:** 137–142.
47. Kuroda, M.A. & J.P. Leburton. 2006. Joule heating induced negative differential resistance in freestanding metallic carbon nanotubes. *App. Phys. Lett.* **89:** 103102.
48. Pop, E., D. Mann, J. Cao, *et al*. 2005. Negative differential conductance and hot phonons in suspended nanotube molecular wires. *Phys. Rev. Lett.* **95:** 155505.
49. Sazonova, V.A. 2006. A tunable carbon nanotube resonator. PhDThesis, Dept. of Physics, Cornell University.
50. Arai, F., C. Ng, P. Liu, *et al*. 2004. Ultra-small site temperature sensing by carbon nanotube thermal probes. *Proc. 4th IEEE Conference on Nanotechnology* 146–148.
51. Avedisian, C.T., R.E. Cavicchi, X. Zhou, *et al.* 2008. High temperature electrical resistance of substrate-supported single walled carbon nanotubes. *Appl. Phys. Lett.* **93**(25): id. 252108, 3 pages.
52. Pop, E., D. Mann, J. Cao, *et al*. 2006. Thermal conductance of an individual single-wall carbon nanotube above room temperature. *Nano Lett.* **6:** 96–100.
53. Kane, A.A., K. Loutherback, B.R. Goldsmith & P.G. Collins. 2008. High temperature resistance of small diameter, metallic single-walled carbon nanotube devices. *Appl. Phys. Lett.* **92:** 083506.